ARTICLES

Orientation and Dynamics of Benzyl Alcohol and Benzyl Alkyl Ethers Dissolved in Nematic Lyotropic Liquid Crystals. ^{2}H NMR and Molecular Dynamics Simulations

H. Ahumada,[†] R. Montecinos,[†] D. P. Tieleman,[‡] and B. E. Weiss-López*,[†]

Departamento de Química, Facultad de Ciencias, Universidad de Chile, Casilla 653, Santiago, Chile, and Department of Biological Sciences, University of Calgary, Calgary, Alberta T2N 1N4, Canada

Received: December 22, 2004; In Final Form: April 25, 2005

Most drugs have to cross cell membranes to reach their final target. A better understanding of the distribution, interactions, and dynamics of biologically active molecules in model bilayers is of fundamental importance in understanding drug functioning and design. ^{2}H NMR quadrupole splittings ($\Delta\nu_Q$) and longitudinal relaxation times (T_1) from the aromatic ring of benzyl alcohol-d_5 (C_0), a commonly used anesthetic, and a series of linear alkyl benzyl-d_5 ethers with chain lengths from 1 to 12 carbon atoms (C_1-C_{12}), were measured. The molecules were dissolved in a nematic discotic lyotropic liquid crystal solution made of tetradecyltrimethylammonium chloride (TTAC)/decanol (DeOH)/NaCl/H_2O. Values of $\Delta\nu_Q$ and T_1 from 1,1-dideuteriodecanol (15% enriched) and DHO (H_2O with 0.2% D_2O) were also measured. $\Delta\nu_Q$ of DeOH and DHO remained constant throughout the series. The value of $\Delta\nu_Q$ of the para position of the ring ($\Delta\nu_p$) in C_1 is 30% smaller than the $\Delta\nu_p$ of C_0. This is attributed to the existence of an H-bond between the alcohol hydroxyl proton and the solvent, which influences the average orientation of the ring. The relaxation data show that $T_{1o,m}$ is always longer than T_{1p} and both decrease with the increase in alkyl chain length. Molecular dynamics simulations of the experimentally studied systems were performed. The aggregate was represented as a bilayer. The distribution, average orientation, and order parameters of the aromatic ring of the guest molecules in the bilayer were examined. Rotational correlation functions of all the C−D bonds and the OH bond from H_2O were evaluated, allowing an estimate of the correlation times and T_1. According to these results all spins relax in extreme narrowing conditions, except DeOH. Experimental and calculated T_1 values differ at most by a factor of 3. However, the order of magnitude and the observed trends are well reproduced by the calculations. The aromatic ring of C_0 possesses a unique average orientation in the bilayer. For the ether series, the orientation is modified and the C_2 symmetry axis of the aromatic ring is exchanging between two orientations averaging the quadrupole splittings from the ortho and meta positions. The simulation supports the existence of an H-bond between C_0 and the solvent not found in the ethers, which should be responsible for the observed differences.

Introduction

The motivation to study the distribution, orientation, and dynamics of biologically active molecules dissolved in anisotropic organized molecular systems arises from the fact that most drugs have to cross cell membranes to reach their final target. A deeper understanding of these processes is of fundamental importance in drug activity and design. A broad range of experimental and theoretical methodologies, such as ^{2}H NMR quadrupole splitting, relaxation time measurements, and molecular dynamics (MD) simulations, among others, have been used to study different aspects of these assemblies.[1−11]

The capabilities of modern microcomputers allow MD simulations of tens of thousands of atoms on a nanosecond time scale to be performed on a desktop PC.[12,13] These calculations, despite the simplicity of the model, provide a detailed description of the system at the atomic level, and in different instances have proved to be very helpful in the interpretation of experimental results.[14,15]

Benzyl alcohol combined with epinephrine has anesthetic capabilities and has been used in surgery as an alternative to lidocaine−epinephrine mixtures, which sometimes lead to allergic reactions. Unmixed it is used as local anesthetic for brief superficial skin procedures.[16,17] It has also been used as a preservative and cosolvent in injectable formulations of nonsteroidal anti-inflammatory drugs, such as diclofenac and piroxicam, as well as in vitamin B complex injection solutions.[18] In this work, we have investigated the interactions between benzyl alcohol and derivatives with a discotic nematic lyotropic liquid crystal, a lipid model of cell membranes. We measured ^{2}H NMR quadrupole splittings ($\Delta\nu_Q$) and longitudinal relaxation times (T_1) of benzyl alcohol-d_5 (C_0) and a series of linear alkyl benzyl-d_5 ether derivatives, ranging from 1 to 12 carbon atoms in the aliphatic chain (C_1-C_{12}). All the molecules in the series

[†] Universidad de Chile.
[‡] University of Calgary.

10.1021/jp0441590 CCC: $30.25
Published on Web 07/09/2005

were dissolved in a nematic discotic lyotropic liquid crystal solution made of tetradecyltrimethylammonium chloride (TTAC)/decanol (DeOH)/NaCl/H_2O. Values of $\Delta\nu_Q$ and T_1 from 1,1-dideuteriodecanol (15% DeOH-d_2 enriched DeOH) and DHO (0.2% D_2O enriched H_2O) were also measured. This type of liquid crystal spontaneously orients with the symmetry axis of the disk perpendicular to the direction of the magnetic field. MD simulations of most experimentally studied systems, represented as bilayers, were performed using the program package GROMACS.[12,13] The distribution, average orientation, order parameters, rotational correlation functions, correlation times, and ^{2}H NMR T_1 relaxation times were estimated from the trajectories. This work constitutes a test of the capabilities of the employed potential functions to properly represent the location and dynamics of the aromatic ring of the guest molecules dissolved in the aggregate.

Materials and Methods

NMR and Sample Preparation. TTAC was prepared from TTAB (Aldrich) using a previously reported methodology.[19] Benzyl alcohol-d_5 (99.5%) was obtained from Aldrich, and the ether-d_5 series was prepared following a standard methodology.[20] DeOH-d_2 was prepared by reduction of ethyl decanoate ester by $LiAlD_4$. The samples were prepared by dissolving 3.64 g of TTAC, 1.14 g of NaCl, and 760 μL of DeOH in 10 mL of H_2O. After mixing, to form the liquid crystal solution, between 5 and 12 μL of benzyl alcohol or ether was added to 0.7 mL of the above solution, depending on molecular weight. The samples were homogenized, degassed using three freeze−pump−thaw cycles, and allowed to equilibrate 4 days. To test for the integrity of the mesophase in the different samples, the H_2O contained 0.2% D_2O, and the DeOH was 15% enriched with DeOH-d_2.

T_1 and $\Delta\nu_Q$ from the aromatic rings of the guest molecules, from DHO, and from DeOH-d_2 were measured in a Bruker Avance 400 NMR spectrometer at 300 K, using a broad-band probe tuned to the deuterium frequency (61.4 MHz). The 90° ^{2}H pulse was 19 μs, and 2048 transients were accumulated for each point in the relaxation curve. A time delay of 1.5 s between transients was employed to restore the Boltzmann distribution. A spectral window of 30 kHz was used for all samples and the transients stored in 16 kB files. Zero filling was applied to obtain a digital resolution of 1 Hz. The T_1 values were measured employing the T1IR pulse sequence, and the quadrupole splittings were measured directly from the fully relaxed spectrum. The errors were estimated from measurements of $\Delta\nu_Q$ and T_1 in three independently prepared samples of C_0. For $\Delta\nu_Q$ they are ±5 Hz for ortho and meta positions, ±10 Hz for the para position, ±1 Hz for DHO, and ±25 Hz for DeOH-d_2. Errors in T_1 were ±4 ms for ortho and meta positions and ±6 ms for the para position. Errors in T_1 of DHO (±23 ms) and DeOH-d_2 (±10 ms) correspond to the standard deviations from the averages of all samples.

Molecular Dynamics. The starting structures of TTA^+, DeOH, and all the guest molecules were constructed using the program Hyperchem (Hypercube Inc., Gainesville, FL). All bilayer setups, trajectory calculations, and analyses were performed using the software package GROMACS, v 3.0.[12,13] The VMD[21] program was employed for the visualization of trajectories and molecular graphics.

Most of the parameters for the potential function, namely bond stretchings, angle bendings, torsions, out-of-plane bendings, and Lennard-Jones, for most atoms were obtained from the GROMOS[22,23] force field. The Lennard-Jones potential for aliphatic chains was evaluated using the parameters of Berger et al.[24] The parameters employed for the deuterium atoms of the rings were the GROMOS parameters for hydrogen, except that the mass was doubled.

The hydrogen atoms in the aliphatic chains were not explicitly represented; instead, the united atom approximation was employed. The charges of all the molecules were obtained from 6-31G* ab initio full geometry optimization calculations followed by MK fitting.[25] The Ryckaert−Bellemans[26] periodic potential function was employed to calculate the torsional energy for aliphatic chains. LINCS[27] was used to constrain the bond lengths of the surfactant chains, and SETTLE[28] was used to restrict the structure of the water molecules. The SPC model was employed for water.[29] A 1 nm cutoff was used for the Lennard-Jones potential and the real space electrostatic interactions. Long-range electrostatic interactions were calculated using PME.[30,31] The update of the neighbor list was performed every 10 time steps. To maintain the temperature and pressure at constant values of 300 K (water, salt, surfactant, and guest molecules coupled separately) and 1 bar, respectively, we used the Berendsen weak coupling algorithm,[32] with time constants of 0.1 and 1 ps for temperature and pressure, respectively. The time step in all simulations was 2 fs. All the calculations were performed in a cluster of Pentium processors.

A unit cell containing two tetradecyltrimethylammonium ions, TTA^+, and one central decanol, all with the alkyl chain in the fully extended 6-31G* minimum energy conformation, was built. The unit cell was copied 4 times in the *X*-direction and 12 times in the *Y*-direction. The generated monolayer, containing 96 TTA^+ ions and 48 DeOH, was displaced 1.7 nm in the *Z*-direction, copied, and rotated 180° around the *Y*-axis to generate the desired bilayer. This system was placed in a rectangular box of dimensions 6.5 × 7.1 × 6.1 nm^3, with periodic boundary conditions in all directions. It contained 4192 SPC[29] water molecules, 288 Na^+ ions, and 480 Cl^- ions. The energy of the system was minimized to avoid bad contacts. The final minimized system was used as the starting structure for 11 simulations with three guest molecules of C_0−C_3, C_5−C_{10}, and C_{12} each. In all cases two guest molecules were placed at the water/surfactant interface and one in the aqueous phase. The energy of each system was minimized again, and the dynamics simulation was allowed to run for 10 ns. All further analysis in this work was performed on the last 5 ns of trajectory.

^{2}H NMR. A brief introduction to longitudinal relaxation of quadrupolar nuclei is provided here since it will be used later. Longitudinal magnetic relaxation of nuclei with spin quantum number $I \geq 1$ is dominated by the quadrupolar interaction. Due to molecular reorientation in the magnetic field, the elements of the quadrupolar coupling tensor are random functions of time, inducing relaxation. The theory relates T_1 to the rotational correlation time of the electric field gradient experienced by the nucleus, τ_c, according to eq 1.[33]

$$1/T_1 = (3/80)(1 + \eta^2/3)[(2\pi eQ/h)(\partial^2 V/\partial z^2)]^2\{J(\omega_o) + 4J(2\omega_o)\} \quad (1)$$

In this work, we assume that the direction of the electric field gradient is the direction of the C−D or O−D σ bonds. In eq 1 η is the asymmetry parameter of the electric field gradient, 0.05 for aromatic C−D.[34] For aliphatic C−D bonds and the O−D bond of water, we assume $\eta = 0.00$. The term in square brackets is the quadrupolar coupling constant in angular frequency units. Reported values of the quadrupole coupling constants are 185 kHz for the aromatic C−D bond,[34] 167 kHz for the aliphatic C−D bond,[35] and 308 kHz for the water O−D bond.[36] ω_o is

the Larmor frequency, and $J(\omega_o)$ is the spectral density at frequency ω_o. Assuming that the rotational correlation function is a single exponential decay, the spectral density becomes

$$J(\omega_o) = 2\tau_c/(1 + \omega_o^2\tau_c^2) \quad (2)$$

Here, τ_c is the rotational correlation time of the electric field gradient, along the C−D or O−D σ bonds. Using the average correlation times, which can be estimated from the MD trajectories, along with the reported values of the coupling constants and η, T_1 values can be calculated. The use of eq 2 to calculate the spectral density can be justified in terms of the rotational correlation functions calculated from the MD simulation. The calculated correlation functions of the guest molecules were all satisfactorily fitted by a single exponential decay function (see Figure 6).

Assuming that the asymmetry parameter of the electric field gradient experienced by the D atom in the C−D bond is negligible, the order parameter of a given C−D bond, S_{CD}, is proportional to the observed quadrupole splitting, $\Delta\nu_{CD}$, according to eq 3.[37]

$$\Delta\nu_{CD} = (3/2)AS_{CD} \quad (3)$$

Here A is the quadrupole coupling constant. Since the sign of the coupling is unknown, only the absolute value of the order parameter can be calculated. The order parameter is defined by eq 4.[37]

$$S_{CD} = (1/2)\langle 3\cos^2(\vartheta - 1)\rangle \quad (4)$$

ϑ is the angle formed by the principal axis of the electric field gradient, considered to be the C−D bond, and the magnetic field. The average is taken over all possible orientations of the bond. The same interaction can be represented in terms of the orientation of the bilayer normal with respect to the field, and the orientation of the C−D bond with respect to the bilayer normal:[6]

$$\Delta\nu = (3/2)AS'_{CD}P_2(\cos\Omega) \quad (5)$$

Here S'_{CD} is the order parameter of the C−D bond relative to the bilayer normal, $P_2(\cos\Omega)$ is the order parameter of the bilayer normal relative to the magnetic field, and Ω is the angle between the bilayer normal and the magnetic field. In the present case the average value of Ω is 90°, and the value of $P_2(\cos\Omega)$ is −1/2. Therefore the transformation between both representations is straightforward.

Results

^{2}H NMR. Figure 1 shows the T1IR stacked plot of spectra for the determination of T_1 and $\Delta\nu_Q$ of C_6. Values of $\Delta\nu_Q$ were measured directly from the fully relaxed spectrum. The largest splitting arises from DeOH-d_2, the next smaller splitting from ortho and meta positions of the ring, and the less intense doublet from the para position of the ring. The most intense doublet with the smallest splitting arises from DHO. The splittings from ortho and meta positions were resolved only for sample C_0. For the ether series only one splitting was observed, $\Delta\nu_{o,m}$. This observation strongly suggests an averaging of the splittings induced by some dynamic process present only in the ethers. Figure 2 is a plot of all the measured quadrupole splittings vs the alkyl chain length. The approximately constant values observed for the quadrupole splittings of DHO and DeOH-d_2 indicates that the mesophase remains unchanged in all the samples.

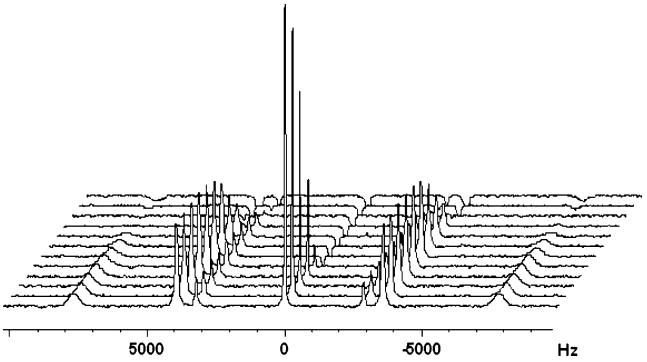

Figure 1. Stack plot of the T1IR experiment obtained from sample C_6. The delays between the 180° and 90° pulses, in seconds, are 1.2, 0.8, 0.5, 0.3, 0.2, 0.12, 0.08, 0.05, 0.035, 0.02, 0.01, and 0.001.

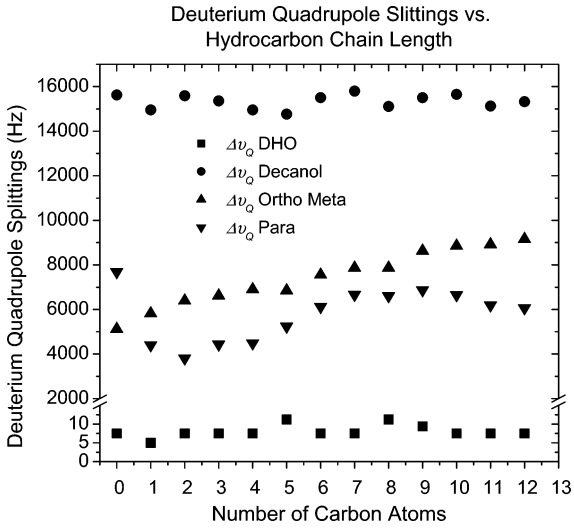

Figure 2. Experimental quadrupole splittings of all deuterium nuclei measured in this work.

The calculations of T_1 were performed using the integrals from the peaks in the right half of the spectra. The integral of both peaks was used for water, and the integral of ortho plus meta peaks was used for C_0. Table 1 shows all the values of $\Delta\nu_Q$ and T_1 measured in this work, except the T_1 of DHO and DeOH-d_2, which were more or less constant with average values of 91 ± 10 and 326 ± 23 ms, respectively. The order parameters for all C−D bonds of the guest molecules, with respect to the bilayer normal, S'_{CD}, were calculated from the splittings, and they are shown in Table 1.

Molecular Dynamics. Molecular dynamics simulations were performed for all the experimentally studied systems, except C_4 and C_{11}. Figure 3 shows a snapshot of system C_6 after 7 ns of trajectory. Three guest molecules were deposited in each box, two at the interface and one in the aqueous region. In most cases the molecule originally positioned in the aqueous region relocated into the aggregate very late in the trajectory, but some never did, despite the fact that they were significantly hydrophobic. Apparently they never reached equilibrium and their rotational correlation functions could not be satisfactorily fitted by a single exponential decay. Therefore, only the two molecules positioned in the interface or the interior of the aggregate were used in further calculations. Longer trajectory calculations seem to be necessary to solve this problem.

TABLE 1: Experimentally Determined Values of $\Delta\nu_Q$, T_1, and Order Parameters Relative to the Bilayer Normal, S', for Ortho, Meta, and Para Positions of Benzyl Alcohol-d_5 and the Series of Ethers-d_5[a]

	quadrupole splittings (Hz)				relaxation times (ms)				order parameters	
	DHO	DeOH	$\Delta\nu_{o,m}$	$\Delta\nu_p$	DHO	DeOH-d_2	$T_{1o,m}$	T_{1p}	$\lvert S'_{o,m}\rvert$	$\lvert S'_p\rvert$
C_0	7.5	15 620	5096 4961	7687	301	103	50	31	0.0370	0.0554
C_1	5.0	14 950	5820	5320	293	98	52	33	0.0420	0.0384
C_2	6.0	15 592	6392	3804	301	77	45	32	0.0460	0.0274
C_3	7.5	15 360	6617	4434	285	81	43	29	0.0476	0.0320
C_4	7.5	14 950	6900	4486	347	78	46	31	0.0498	0.0324
C_5	11.2	14 760	6850	5231	332	99	46	31	0.0494	0.0378
C_6	7.5	15 500	7553	6122	335	81	45	28	0.0544	0.0442
C_7	7.5	15 800	7870	6665	343	93	41	27	0.0568	0.0480
C_8	11.2	15 110	7870	6598	336	86	41	27	0.0568	0.0476
C_9	9.4	15 505	8635	6864	349	97	36	21	0.0622	0.0494
C_{10}	7.5	15 650	8856	6643	343	94	37	19	0.0638	0.0478
C_{11}	7.5	15 124	8917	6192	345	101	38	19	0.0642	0.0446
C_{12}	7.5	15 320	9155	6059	336	102	34	21	0.0660	0.0436

[a] The errors in $\Delta\nu_Q$ were estimated to be ±5 Hz for the ortho and meta positions, ±10 Hz for the para position, ±1 Hz for DHO, and ±25 Hz for DeOH-d_2. The errors in T_1 were ±4 ms for the ortho and meta positions and ±6 ms for the para position.

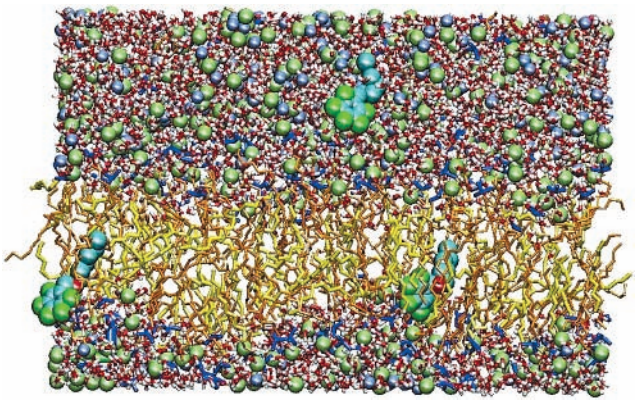

Figure 3. Snapshot of system C_6 after 7 ns of trajectory. The methylammonium headgroups are blue and the hydrocarbon tails are orange; oxygen atoms of DeOH and H_2O are red, hydrogen atoms of DeOH and H_2O are white, and the chain of DeOH is yellow. Sodium ions are blue, and chloride ions are green. The carbon atoms of the ether are light blue, and the deuterium atoms are green.

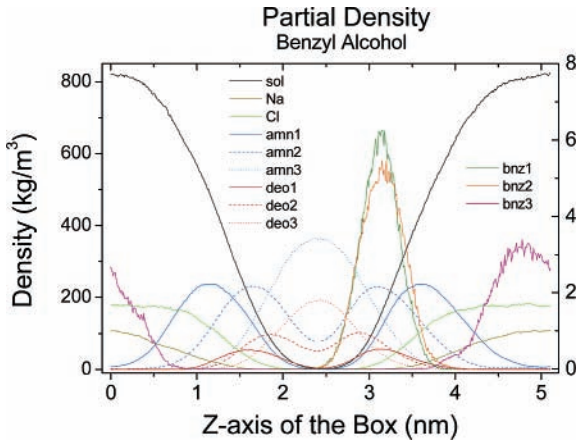

Figure 4. Density profile along the *Z*-axis of the box for all components of sample C_0. For clarity DeOH and TTA^+ were divided into three groups. Details of the divisions appear in the text. The curves correspond to the position of the center of mass of each group, molecule, or ion. The scale on the right applies to benzyl alcohol molecules, and the one on the left applies to the others.

Density profiles along the *Z*-axis of the box for all components of the mesophase, including the three guest molecules, were calculated. Figure 4 shows the density profile of sample C_0. The scale on the right applies to benzyl alcohol molecules and the one on the left to all other components. The behavior of the mesophase components, observed in this figure, is representative of the density profile of the mesophase components in all samples. For clarity, DeOH and TTA^+ were divided into three fragments. In the case of DeOH, the hydroxyl group and the first methylene group constitute the first fragment (deo1), the central hydrophobic region is the second (deo2), and the last four carbon atoms of the chain are the third (deo3). For TTA^+ the first fragment is the ammonium headgroup and the first two methylene groups (amn1), the second is the central portion of the chain (amn2), and the third is the last six carbon atoms of the chain (amn3). The curves in the plot correspond to the position of the center of mass of each group, molecule, or ion. Clearly, DeOH and TTA^+ molecules constitute the bilayer, oriented with the headgroup toward the solvent and the alkyl chain to the interior. The DeOH headgroup is located, on average, about 0.5 nm more to the interior of the bilayer than the TTA^+ headgroup, and the thickness of the interface, according to a previous definition,[38] is about 1.5 nm. These two properties were estimated for an oblate model of the aggregate with the same composition, and the results were 0.3 and 1.7 nm, respectively.[1] The difference is possibly due to the larger curvature of the aggregate's surface, as compared to the bilayer model, which widens the interface and allows the DeOH headgroups to move closer to the water. It is also apparent that one benzyl alcohol is significantly displaced toward the aqueous region and the other two remain at the interface, close to the hydrophobic core. Furthermore, it is observed that the molecule located in the aqueous phase displays a significantly larger displacement than the two located at the interface. The same information about the location and distribution of the aromatic ring of one of the guest molecules initially located at the interface was obtained for all calculated systems. The results of these calculations appear in Figure 5. In this figure the *Y*-axis of the plot corresponds to the *Z*-axis of the box. The dotted line is the limit between the interface and the aqueous region, the dashed line is the limit between the interface and the hydrophobic core, and the solid line denotes the center of the bilayer. The dots in this plot correspond to the maximum of the aromatic ring density profiles, the most probable location, and the vertical line denotes the full amplitude of the distribution. The presence of more than one dot for a given molecule indicates the presence of two maxima in the density profile.

TABLE 2: Average Rotational Correlation Times, τ_c (ps), Values of T_1 (ms) from the Aromatic Ring, Average Angle between the Vector Perpendicular to the Ring Plane and the Bilayer normal (θ_1, deg), Average Angle between the C_2 Symmetry Axis of the Ring and the Bilayer normal (θ_{2a} and θ_{2b}, deg), and Order Parameter from the para C−D Bond[a]

	correlation times		relaxation times		average angles			
	$\tau_c^{o,m}$	τ_c^{p}	$T_{1o,m}$	T_{1p}	$\langle\theta_1\rangle$	$\langle\theta_{2a}\rangle$	$\langle\theta_{2b}\rangle$	order parameter $\lvert S_p'\rvert$
C_0	11.0 ± 2.4	25.1 ± 0.9	179.0	79.5	105 ± 39	115 ± 36		0.0318 ± 0.45
C_1	10.3 ± 0.4	25.8 ± 8.4	192.2	76.5	81 ± 38	103 ± 40	71 ± 41	0.0222 ± 0.45
C_2	10.8 ± 1.8	25.4 ± 3.4	182.0	77.7	85 ± 39	117 ± 36	64 ± 36	0.0284 ± 0.45
C_3	16.5 ± 2.0	66.5 ± 17	119.8	29.7	84 ± 40	129 ± 44	68 ± 43	0.0891 ± 0.43
C_5	16.6 ± 1.6	66.6 ± 16	119.2	29.7	85 ± 38	118 ± 42	51 ± 43	0.0805 ± 0.44
C_6	16.8 ± 1.7	55.0 ± 4.1	117.1	35.9	87 ± 37	115 ± 38	76 ± 37	0.0602 ± 0.45
C_7	11.8 ± 1.0	87.6 ± 51	166.7	22.6	87 ± 38	133 ± 44	71 ± 45	0.0841 ± 0.46
C_8	19.3 ± 5.5	99.4 ± 52	102.0	19.9	86 ± 40	140 ± 46	73 ± 45	0.0863 ± 0.45
C_9	20.5 ± 3.1	74.7 ± 7.5	96.3	26.5	87 ± 40	137 ± 42	71 ± 41	0.0892 ± 0.43
C_{10}	16.3 ± 2.9	61.2 ± 19	121.4	32.2	97 ± 38	141 ± 46	58 ± 45	0.1019 ± 0.45
C_{12}	24.2 ± 9.1	80.6 ± 15	81.6	24.5	95 ± 37	135 ± 44	56 ± 43	0.0824 ± 0.47

[a] All values were obtained from the GROMACS trajectories. [b] The values of $\tau_c^{o,m}$ are the average of the ortho and meta positions for the two molecules considered, and the associated error is the standard deviation from that average. The same procedure was employed for the para position.

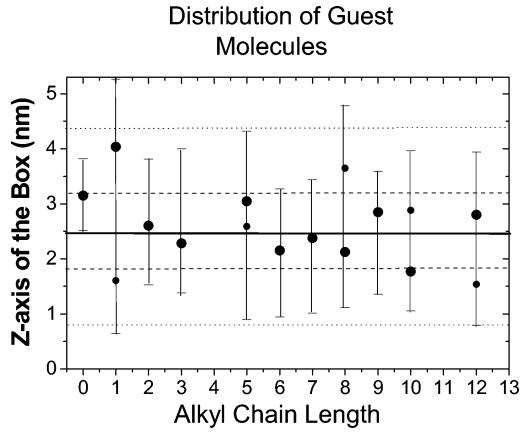

Figure 5. Distribution of one of the guest molecules initially located at the interface along the *Z*-axis of the box, for all calculated systems. The dotted line is the limit between the interface and the aqueous region, the dashed line is the limit between the interface and the hydrophobic core, and the solid line denotes the center of the bilayer. The dots in this plot correspond to the maxima of the aromatic ring density profiles, the most probable location, and the vertical line denotes the full amplitude of the distribution. The presence of more than one dot for a given molecule indicates the presence of two maxima in the density profile. The size of the dot is proportional to the magnitude of the maximum; i.e., the largest dot corresponds to the most probable location.

The size of the dot is proportional to the magnitude of the maximum; i.e., the largest dot corresponds to the most probable location.

Rotational correlation functions of all C−D bonds of the aromatic rings, DeOH-d_2, and the O−H bond of H_2O were calculated from the trajectories. All the functions corresponding to the guest molecules were fitted to a single exponential decay, and an estimation of the τ_c values was obtained. This result supports the use of eq 2 to calculate the relaxation times. The rotational correlation function for the C−D bond of DeOH-d_2 was not satisfactorily fitted by a single exponential decay. Figure 6 shows the rotational correlation function of the ortho C−D bond obtained from the trajectory of one C_0 molecule and the corresponding single exponential decay fit. The behavior of the rotational correlation functions of the guests seems to be well represented by a single exponential decay function. Since experimentally only one splitting is observed for most ortho and meta deuterons, the values of τ_c from these positions were all averaged for both molecules inside the bilayer. Similarly, the average τ_c from both para positions was considered. Table

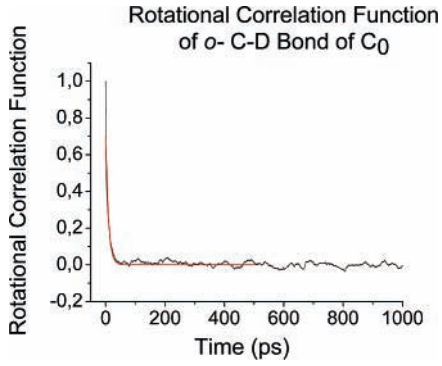

Figure 6. Rotational correlation function of C−D bond from ortho position of sample C_0. The black trace is the correlation function obtained from the trajectory, and the red trace is the single exponential decay fitting.

2 lists all the calculated average values of τ_c, their estimated errors, and the values of the calculated T_1 using eq 1.

Two angles are necessary to describe the average orientation of the aromatic ring in the bilayer. For this purpose we defined θ_1 as the angle between the vector perpendicular to the aromatic ring plane and the bilayer normal, and θ_2 as the angle between the local C_2 symmetry axis of the ring and the bilayer normal. The vector pointing from carbon 1 to carbon 4 of the ring defines the C_2 symmetry axis. For benzyl alcohol both angles are single valued; however, all the ethers displayed two possible values for the second angle, designated by θ_{2a} and θ_{2b}. All the calculated average angles are displayed in Table 2.

The order parameters of the para C−D bond of the rings with respect to the direction of the bilayer normal were also calculated from the trajectories. The time scale of a few nanoseconds for the order parameter calculations is clearly insufficient when compared with the time scale of the experiment, and this seems to be reflected in the large errors displayed. Despite the fact that these calculated order parameters should be taken with care, the numbers obtained appear in Table 2.

Discussion

NMR. The location and orientation of benzyl alcohol in anisotropic media has been examined before, experimental and theoretically. Some years ago, a ^{13}C NMR chemical shift and UV spectroscopy study about the distribution of C_0 in unilamellar vesicles of egg yolk phosphatidylcholine was published.[39] Their results indicate that benzyl alcohol is located at

the interface, close to the carbonyl group of the phospholipids, oriented with the methylene group toward the hydrophobic region of the bilayer. Later, we measured the quadrupole splittings and estimated the order parameters of the aromatic ring of the series C_0-C_{12}, dissolved in anionic nematic lyotropic liquid crystals.[11] The results suggested that C_0 was also located at the bilayer interface, but with a different orientation of the ring relative to the previous observation in vesicles.[39] Evidence was also found to support the existence of an H-bond between C_0 and the solvent.

In the present study the magnitude of the quadrupole splittings from the aromatic ring indicates that all the guest molecules are associated to the aggregate. The splitting from the para position, $\Delta\nu_p$, is related to the order parameter of the C_2 symmetry axis of the ring, collinear with the para C−D bond, and should not be affected by motions around the phenyl torsional coordinate. The four atoms defining the phenyl torsional coordinate are the oxygen atom, the methylene carbon directly bonded to the aromatic ring, and carbons 1 and 2 of the ring. On the other hand, $\Delta\nu_{o,m}$ should be affected by both motions, the oscillations of the phenyl torsional coordinate and the motions of the symmetry axis of the ring. The behavior of $\Delta\nu_p$ and $\Delta\nu_{o,m}$ along the series should reflect the process of incorporation of the aromatic ring into the aggregate as a consequence of the increasing hydrophobicity of the alkyl chain. Figure 2 shows that $\Delta\nu_{o,m}$ progressively increases with the increase of the aliphatic chain length. This is due to the progressive incorporation of the ring further into the interior of the aggregate, increasing restrictions to the torsional motion and due to the increase in molecular mass. The behavior of $\Delta\nu_p$ is more interesting: it decreases by about 30% on going from C_0 to C_1, remains more or less constant from C_1 to C_4, and increases from C_5 to C_7, to finally reach an approximately constant value from C_8 to C_{12}. As a consequence of the large decrease in $\Delta\nu_p$, a crossing between the splittings of C_0 and C_1 is observed. This crossing can be attributed to two factors: (1) a modification in the reorientational dynamics of the C−D bond from the para position, or (2) a change of its average orientation, or both. If the origin of the decrease was a difference in the reorientational dynamics of the ring, it should modify the rotational correlation time and would be reflected in the values of T_{1p}. An inspection of Table 1 reveals that the values of T_{1p} for C_0 and C_1 are the same, within experimental error, and no crossing is observed. This strongly suggests that the decrease in the splitting should be mostly due to modifications in the average orientation of the ring. This modification could have its origin in the existence of an H-bond between the proton of the alcohol and the solvent, precluded in the ethers. The order parameters from the para C−D bond relative to the bilayer normal (Table 1) also show a decrease of about 30% on going from C_0 to C_1. This decrease of S'_p going from C_0 to C_1 is qualitatively reproduced by the order parameters calculated from the MD trajectories (Table 2), despite the little confidence in these numbers.

The results of $\Delta\nu_p$ for the rest of the series seem to indicate that an alkyl chain of five carbons is necessary to effectively start modifying the degree of alignment of the ring in the interior of the aggregate. Longer chain derivatives should progressively increase their alignment, and the observed tendency in $\Delta\nu_p$ seems to reflect this process. For alkyl chain lengths of eight or nine carbon atoms or longer, the guest molecule seems to be completely incorporated as an integral part of the aggregate, with essentially the same orientation and dynamics. Further increase in hydrophobicity no longer modifies the behavior of $\Delta\nu_p$.

The relaxation data from the aromatic rings reveals that $T_{1o,m}$ is always longer than T_{1p}, and both decrease with the increase in the alkyl chain length (Table 1). This observation can also be rationalized in terms of the motions of the ring. As mentioned before, the phenyl torsional motion does not affect the dynamics of the para position, making the corresponding correlation time longer and consequently T_{1p} shorter. The decrease of both $T_{1o,m}$ and T_{1p} with the increase in alkyl chain length is expected from a decrease in overall motion due to the incorporation and alignment phenomena, and the increase in molecular weight.

Molecular Dynamics. Several years ago, a 1 ns MD trajectory calculation of three C_0 molecules dissolved in a phospholipid bilayer was published.[40] However, in that work all the guest molecules were originally positioned at the interior of the bilayer and did not show significant displacement along the normal to the interface. Perhaps the short length of the simulation did not allow the molecules to diffuse into the interface.

From Figure 5 it is seen that in the present case C_0 remains at the limit between the interface and the hydrophobic core, with the smallest displacement from the most probable location. C_1 also remains at the interface. However, C_1 is the guest molecule most widely distributed along the *Z*-axis of the bilayer. In fact, it is the only guest able to cross the bilayer from side to side in the simulation. Ethers C_2-C_7 are mainly located in the hydrophobic core of the bilayer displaying only one maximum, except for ether C_5, which displays a small shoulder but is also located in the hydrophobic core. This suggests that the rings of these molecules reside most of the time near the center of the bilayer, with no preferential orientation inside the aggregate. On the other hand, rings from ethers C_8-C_{12} display two maxima, both positioned near the limits between the interface and the hydrophobic core. This result suggests that these molecules should form an integral part of the aggregate, with the aromatic ring in the interface and the alkyl chain toward the interior of the hydrophobic core. Ether C_9 is the exception with only one maximum; however, it is also located in the same region of the interface. Figure 5 seems to qualitatively represent the tendency manifested by the quadrupole splittings of the ring, at least partially. A significant decrease of $\Delta\nu_p$ going from C_0 to C_1 is consistent with the significantly larger displacement of C_1 along the normal to the bilayer when compared with C_0, in the same amount of time. Constant values of the splittings for the largest derivatives, C_9-C_{12}, suggest that all these molecules should be located in the same region of the aggregate, as displayed in Figure 5. Therefore both theory and experiment suggest that the long chain derivatives should be completely incorporated as an integral part of the aggregate, i.e., with the aromatic ring oriented toward the interface and the aliphatic chain to the interior. Differences between theory and experiment could arise from the lack of a complete sampling of the system, due to the limited extension of the simulation.

The two angles that define the average orientation of the aromatic rings in the bilayer are displayed in Table 2. These values indicate that benzyl alcohol presents a unique orientation in the bilayer. On the other hand, the symmetry axis of the aromatic ring of all the ethers in the series is moving between two possible orientations. The C_2 symmetry axis of benzyl alcohol makes an angle of 115° with respect to the bilayer normal, and the angle decreases to either 103° or 71° in ether C_1. The vector perpendicular to the ring plane of benzyl alcohol forms an angle of 105° with the bilayer normal, and the angle decreases to 81° for ether C_1. These variations represent a significant modification in the average orientation of the ring and should be responsible for the observed variations in

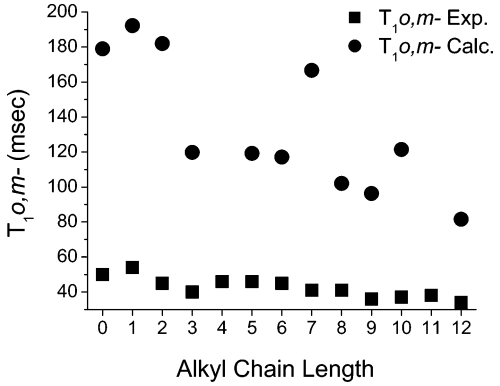

Figure 7. Experimental and calculated values of $T_{1o,m}$.

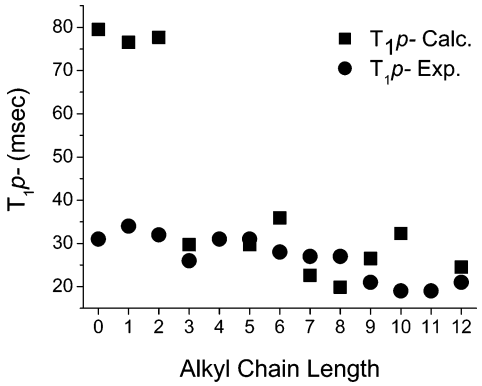

Figure 8. Experimental and calculated values of T_{1p}.

quadrupole splittings. For the ethers, the values of θ_1 and θ_{2a} increase progressively with the increase in alkyl chain length, up to maximum values of about 97° and 148°, respectively. The values of θ_{2b} remained more or less constant along the series. The dynamic process responsible for the exchange of the symmetry axis of the ring between two different sites should be responsible for the averaging observed in the quadrupole splittings of ortho and meta positions of the ether series.

Despite the large uncertainty in the calculated order parameters, the difference between C_0 and C_1 is qualitatively reproduced by the MD calculations. The large errors displayed by these values probably reflect the uncertainty in their estimation from nanosecond time scale trajectory averages.

The possibility of an H-bond between C_0 and the solvent was also explored. The distribution of donor−acceptor distances and the number of H-bonds as a function of time were obtained for all simulated systems. The existence of a preferential distance within the magnitude of an H-bond (0.18 nm) and a significant residence time were obtained only for C_0. The residence time and the distance distribution plots of all the ether derivatives show no evidence to support the formation of an H-bond.

Table 2 shows calculated values of τ_c and T_1. All the molecules relax in extreme narrowing conditions ($\omega\tau \ll 1$), except DeOH-d_2. A large dispersion in the calculated values of τ_c is seen from this table, reflecting the difficulty of sampling these correlation functions from a nanosecond scale trajectory. The solvent T_1 was estimated from the fitting of the rotational correlation functions of 10 O−H bonds from H_2O in sample C_6. The obtained average value of τ_c was 3.4 ± 0.7 ps and $T_1 = 210$ ms, about twice the experimental value.

The calculated relaxation times for the aromatic rings are also listed in Table 2. Figures 7 and 8 are plots of the experimental and calculated values of $T_{1o,m}$ and T_{1p}, respectively, as functions of the alkyl chain length. It can be seen that the observed experimental tendencies are well reproduced by the calculations. From Figure 8 it is seen that the calculated values of $T_{1o,m}$ are always overestimated. This may arise from a deficiency of the torsional potential function used for the ring, which could underestimate the torsional force constant, yielding a shorter correlation time.

Conclusions

From the results of this work we conclude that all studied guest molecules are strongly attached to the aggregate. The force field employed in these MD simulations provides a reasonable qualitative description of the distribution, average orientation, and dynamics of the aromatic ring of the guest molecules dissolved in the liquid crystal solution. Both experiment and theory suggest that an aliphatic chain of about eight or nine carbons is sufficiently hydrophobic to completely align the guest molecule inside the aggregate. Remarkably, the ^2H T_1 relaxation times calculated from the trajectories of the aromatic rings reproduce the tendencies observed in the experimental values, despite the possible deficiencies of the force field to represent the dynamics of the aromatic ring. The simulations also provided evidence for the existence of an H-bond between C_0 and the solvent that is not present in the ether series. The rupture of the H-bond, on going from the alcohol to the ethers, should be responsible for a significant modification in the average orientation of the aromatic ring of the ether series. The existence of a dynamic process reorienting the ring symmetry axis averages the quadrupole splittings from ortho and meta positions in the ether series.

Acknowledgment. The authors are pleased to acknowledge financial assistance from Fondecyt, Grants Nos. 1010211 and 7010211. H.A. and R.M. acknowledge Doctoral Fellowships and Thesis Support from Conicyt (AT-4040107) and the Post Graduate Division, Universidad de Chile (PG/40/2003 and PG/45/2003). D.P.T. is a Scholar of the Alberta Heritage Foundation for Medical Research. Work in his group is supported in part by NSERC.

References and Notes

(1) Montecinos, R.; Ahumada, H.; Martínez, R.; Olea, F. A.; Araya-Maturana, R.; Aliste, M. P.; Tieleman, D. P.; Weiss-López, B. E. *Langmuir* **2004**, *20*, 5703−5708.

(2) Johannesson, H.; Furó, I.; Halle, B. *Phys. Rev. E* **1996**, *53*, 4904−4917.

(3) Bemporad, D.; Essex, J. W.; Luttmann, C. *J. Phys. Chem. B* **2004**, *108*, 4875−4884.

(4) Bemporad, D.; Luttmann, C.; Essex, J. W. *Biophys. J.* **2004**, *87*, 1−13.

(5) Mukhopadhyay, P.; Vogel, H. J.; Tieleman, D. P. *Biophys. J.* **2004**, *86*, 337−345.

(6) Brown, M. F.; Thurmond, R. L.; Dodd, S. W.; Otten, D.; Beyer, K. *J. Am. Chem. Soc.* **2002**, *124*, 8471−8484.

(7) Belohorcova, K.; Qian, J.; Davis, J. H. *Biophys. J.* **2000**, *79*, 3201−3216.

(8) Weiss-López, B. E.; Azocar, M.; Montecinos, R.; Cassels, B. K.; Araya-Maturana, R. *Langmuir* **2001**, *17*, 6910−6914.

(9) Solgadi, A.; Meddour, A.; Courtieu, J. *Tetrahedron: Asymmetry* **2004**, *15*, 1315−1318.

(10) Weiss-López, B. E.; Gamboa, C.; Tracey, A. S. *Langmuir* **1995**, *11*, 4844−4847.

(11) Weiss-López, B. E.; Miño, G.; Araya-Maturana, R.; Tracey, A. S. *Langmuir* **2000**, *16*, 4040−4044.

(12) Berendsen, H. J. C.; van der Spoel, D.; van Drunen, R. *Comput. Phys. Commun.* **1995**, *91*, 43−56.

(13) Lindahl, E.; Hess, B.;van der Spoel, D. *J. Mol. Model.* **2001**, *7*, 306−317.

(14) Ahumada, H.; Montecinos, R.; Martínez, R.; Araya-Maturana, R.; Weiss-López, B. E. *J. Chil. Chem. Soc.* **2004**, *49*, 209−213.

(15) Hoff, B.; Strandberg, E.; Ulrich, A. S.; Tieleman, D. P.; Posten, C. *Biophys. J.* **2005**, *88*, 1818−1827.

(16) Bartfield, J. M.; May-Wheeling, H. E.; Raccio-Robak, N.; Lai, S. Y. *J. Emerg. Med.* **2001**, *21*, 375−379.
(17) Wilson, L.; Martin, S. *Ann. Emerg. Med.* **1999**, *33*, 495−499.
(18) Kazemifard, A. G.; Moore, D. E.; Mohammadi, A.; Kebriyaeezadeh, A. *J. Pharmaceut. Biomed.* **2003**, *31*, 685−691.
(19) Sepúlveda, L.; Cabrera, W.; Gamboa, C.; Meyer, M. *J. Colloid Interface Sci.* **1986**, *117*, 460−463.
(20) Weiss-López, B. E.; Saldaño, D.; Araya-Maturana, R.; Gamboa, C. *Langmuir* **1997**, *16*, 4040−4044.
(21) Humphrey, W.; Dalke, A.; Schulten, K. *J. Mol. Graphics* **1996**, *14*, 33−38.
(22) Van Gunsteren, W. F.; Berendsen, H. J. C. *GROMOS Software Package*; Biomos: Nijenborgh 4, 9747AG, Groningen, The Netherlands.
(23) Van Gunsteren, W. F.; Berendsen, H. J. C. *Angew. Chem., Int. Ed. Engl.* **1990**, *29*, 992−1023.
(24) Berger, O.; Edholm, O.; Jhaning, F. *Biophys. J.* **1997**, *72*, 2002−2013.
(25) Besler, B. H.; Merz, K. M.; Kollman, P. A. *J. Comput. Chem.* **1990**, *11*, 431−439.
(26) Ryckaert, J. P.; Bellemans, A. *Faraday Discuss. Chem. Soc.* **1978**, *66*, 95−106.
(27) Hess, B.; Bekker, H.; Berendsen, H. J. C.; Fraaije, J. *J. Comput. Chem.* **1997**, *18*, 1463−1472.
(28) Miyamoto, S.; Kollman, P. A. *J. Comput. Chem.* **1992**, *13*, 952−962.
(29) Berendsen, H. J. C.; Postma, J. P. M.; Gunstere, W. F.; Hermans, J. Interaction Models for Water in Relation to Protein Hydration. In *Intermolecular Forces*; Pullman, B., Ed.; Reidel: Dordrecht, The Netherlands, 1981; pp 331−342.
(30) Darden, T.; York, D.; Pedersen, L. *J. Chem. Phys.* **1993**, *98*, 10089−10092.
(31) Essmann, U.; Perera, L.; Berkowitz, M. L.; Darden, T.; Lee, H.; Pedersen, L. G. *J. Chem. Phys.* **1995**, *103*, 8577−8592.
(32) Berendsen, H. J. C.; Postma, J. P. M.; van Gunsteren, W. F.; Dinola, A.; Haak, J. R. *J. Chem Phys.* **1984**, *81*, 3684−3690.
(33) Abragam, A. *Principles of Nuclear Magnetism*; Clarendon Press: Oxford, 1985; p 314.
(34) Clymer, J. W.; Ragle, J. L. *J. Chem. Phys.* **1982**, *77*, 4366−4373.
(35) Raffard, G.; Steinbruckner, S.; Arnold, A.; Davis, J. H.; Dufourc, E. J. *Langmuir* **2000**, *16*, 7655−7662.
(36) Hansen, M. J.; Wendt, M. A.; Farrar, T. C. J. *Phys. Chem. A* **2000**, *104*, 5328−5334.
(37) Diehl, P.; Khetrapal, C. L. NMR Studies of Molecules Oriented in the Nematic Phase of Liquid Crystals. In *NMR Basic Principles and Progress*; Diehl, P., Fluck, E., Kosfeld, R., Eds.; 1969; Vol. 1, p 16.
(38) Tieleman, D. P.; van der Spoel, D.; Berendsen, H. J. C. *J. Phys. Chem. B* **2000**, *104*, 6380−6388.
(39) Okamura, E.; Nakahara, M. *J. Phys. Chem. B* **1999**, *103*, 3505−3509.
(40) López-Cascales, J. J.; Hernández-Cifre, J. G.; García de la Torre, J. *J. Phys. Chem. B* **1998**, *102*, 625−631.